AIAA 93-0123
The High Resolution Doppler Imager (HRDI) on the Upper Atmosphere Research Satellite

H.J. Grassl, W.R. Skinner, P.B. Hays, M.D. Burrage,
D.A. Gell, A.R. Marshall, D.A. Ortland & V.J. Abreu
The University of Michigan
Ann Arbor, MI

31st Aerospace Sciences Meeting & Exhibit
January 11-14, 1993 / Reno, NV

THE HIGH RESOLUTION DOPPLER IMAGER (HRDI) ON THE UPPER ATMOSPHERE RESEARCH SATELLITE

Heinz J. Grassl, Wilbert R. Skinner, Paul B. Hays, David A. Gell,
Mark D. Burrage, David A. Ortland, Alan R. Marshall, and Vincent J. Abreu
Space Physics Research Laboratory
Department of Atmospheric, Oceanic and Space Sciences
The University of Michigan
Ann Arbor, Michigan

Abstract

The High Resolution Doppler Imager (HRDI) on the Upper Atmosphere Research Satellite is an instrument used to observe winds in the Earth's stratosphere, mesosphere and lower thermosphere. Winds are measured by determining the Doppler shift of emission (mesosphere and lower thermosphere) and absorption (stratosphere) lines of the O_2 Atmospheric ($^1\Sigma$-$^3\Sigma$) band. HRDI is a triple-etalon Fabry-Perot interferometer that has a resolution of ~0.05 cm^{-1} and very good white light rejection. Careful design and calibration has permitted systematic errors in the wind determination in the stratosphere to be less than 10m/s.

I. Introduction

The distributions of most chemical species in the stratosphere are affected by both dynamical and chemical processes. Conversely, the distribution of certain photochemical species, such as ozone, can influence the radiative budget of the stratosphere, affecting temperatures and motions. Satellite remote observations of the stratosphere to date have provided only temperature and constituent measurements. The horizontal winds on a global basis have been deduced from temperature fields by using the thermal wind relationships, which relate the vertical shear of the geostrophic wind components to horizontal temperature gradients. These equations, however, are only a good approximation for large scale, low-frequency, extratropical flows.[1] The High Resolution Doppler Imager (HRDI) on the Upper Atmosphere Research Satellite (UARS) is providing the first direct measurement of the global horizontal wind field in the stratosphere and mesosphere. UARS was launched September 12, 1991 into a 585 km circular orbit inclined 57° to the equator.[2] The spacecraft contains ten instruments designed to study the chemistry and dynamics of the stratosphere and above. Knowledge of the stratospheric wind field will help to determine how transport and mixing influence the ozone budget in the lower stratosphere, and to quantify the mean and eddy circulations associated with observed semi-annual oscillations. In the mesosphere, the wind measurements will help to assess the relative role of turbulent diffusion and bulk advection in accounting for mesospheric tracer budgets.

The goal of HRDI is to measure the vector winds in the stratosphere (15 to 40 km), mesosphere and lower thermosphere (~60-120 km) during the day, and the mesosphere at night (~95 km) to an accuracy of 5 meters/second. In addition to winds, the instrument also determines temperatures, cloud top heights, effective albedo, aerosol phase function and scattering coefficient. The measurement technique[3,4] consists of using the Doppler shift of rotational lines of molecular oxygen along two lines of sight in order to determine the horizontal wind vector. Figure 1 is a schematic illustrating the physical processes involved in the measurement. Depending on the band and atmospheric region, molecular oxygen lines can be observed in either emission or absorption, the latter dominating below ~50 km. Solar radiation incident on the atmosphere is absorbed, exciting molecular oxygen into the $O_2(b^1\Sigma_g^+)$ state. This can occur directly through resonance or photochemical reactions.[5,6] When this process takes place in the mesosphere or above, where quenching effects are small, the O_2 emission lines in the A band of the $(b^1\Sigma_g^+, v'=0 - X^1\Sigma_g^-, v''=0)$ transition are observable. The contribution from emission in the B(1,0) and γ(2,0) bands is much weaker because the excited vibrational states are collisionally quenched into the v'=0 state before the electronic transition takes place.[7-9] Emission in the B and γ bands can thus be ignored in the stratosphere and mesosphere. Below ~50 km electronic quenching $(b^1\Sigma_g^+ - X^1\Sigma_g^-)$ rather than emission dominates the loss process. In this case the photons absorbed are not reemitted, and absorption lines develop in the spectrum. Absorption features in the A (~762 nm, 13120 cm^{-1}), B (~688 nm, 14525 cm^{-1}) and γ (~629 nm, 15900 cm^{-1}) bands can be observed when solar

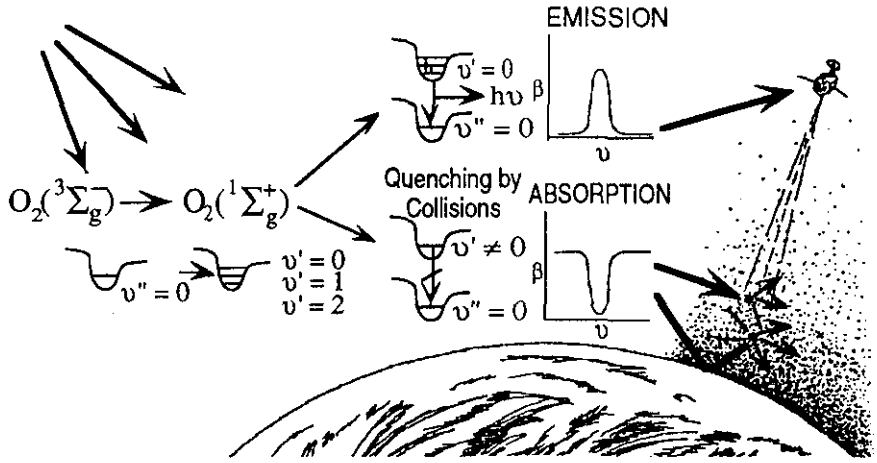

Fig. 1. Schematic illustrating the physical processes involved in the HRDI measurement.

radiation is elastically scattered by molecules (Rayleigh) and aerosols (Mie) into the field of view of the observer. This scattering may occur before or after light is reflected from the surface. The line features generated by the Atmospheric bands (see Ref. 3) are generally quite narrow, with a width of ~0.001 nm (2×10^{-2} cm^{-1}), and lend themselves to the Doppler shift measurement technique.

The HRDI instrument and early results have been discussed elsewhere.[10-15] This paper will review the instrument, discuss some of the important in-flight calibrations, and give examples of the type of data recovery possible. There are a number of atmospheric parameters that can be obtained with HRDI, but this paper will deal exculsively with the recovery of winds.

II. Instrumentation

II.A. Theory of Operation

A horizontal wind speed of 10 m/s, which is typical for the middle atmosphere, causes a Doppler shift of $\sim 2 \times 10^{-5}$ nm (4×10^{-4} cm^{-1}). This small shift requires a high resolution spectrometer with high *sensitivity and very good stability*. The HRDI instrument is a multiple Fabry-Perot interferometer designed to achieve these goals. The Fabry-Perot was chosen because of its large light gathering power and high resolution.[16] Since complete descriptions of the Fabry-Perot interferometer have been given elsewhere[17,18] only an outline is provided here. The Fabry-Perot interferometer is a decepively simple device that consists of two transparent plates that are extremely flat (up to λ/200) and parallel (tilt < 2×10^{-11} rad). The inside surfaces are coated with a relatively high reflectivity coating (~80 to ~95%), that is usually a multilayer dielectric stack. The device is a reasonating cavity which forms Haidinger fringes at an infinite distance from the etalon, which are brought back to some finite distance by the use of imaging optics. The transmittance for an ideal Fabry-Perot etalon is given by the Airy function

$$T(m) = \frac{(1-R)^2}{1-2R\cos(2\pi m)+R^2} \qquad (1)$$

where R is the reflectivity of each plate and m is the order of interference, which in turn is given by

$$m = 2\mu t\nu\cos(\theta) \qquad (2)$$

where μ is the index of refraction of the material between the plates, t the separation between the plates, ν the wavenumber of light, and θ the angle of incidence in the gap. The peak transmittance of such an ideal etalon is 1 and occurs whenever the order of interference is an integer. This can occur for infinite combinations of μ,t,θ, and ν. If we vary only the wavenumber, the separation between peaks at normal incidence is

$$\Delta\nu = 1/(2\mu t) \qquad (3)$$

If m is an integer for the conditions μ=1 (vacuum), $t=t_o$, $\theta=\theta_o=0$ and $\nu=\nu_o$, then in order for m to remain an integer the following condition must be satisfied:

$$\Delta\nu/\nu = \theta^2/2 - \Delta t/t_o. \qquad (4)$$

This illustrates that for spaceflight applications there are two practical methods for scanning a Fabry-Perot interferometer in wavenumber: 1) by looking at different angles through the interferometer, which amounts to viewing different spatial locations at the focal plane of the imaging optics, and 2) by varying the thickness of the etalon gap. Both of these techniques are utilized by HRDI.

The Airy function describes a periodic response as shown in Fig. 2(a). This instrument response is adequate to observe narrow spectral features with a very small background, so that light will be transmitted only through one order. This nearly

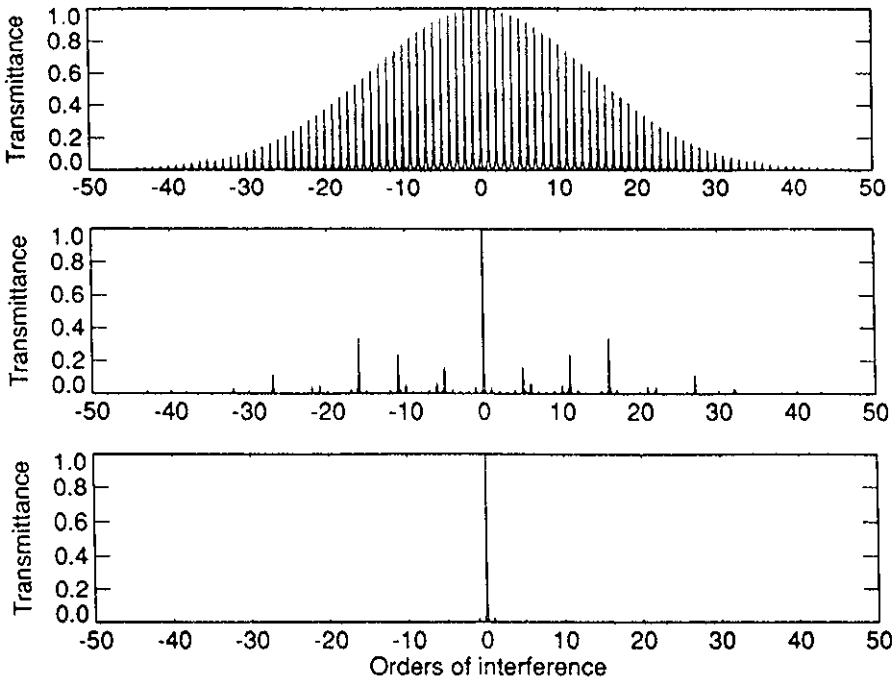

Fig. 2. Illustration of how multiple etalon change the instrument function. (a) Single etalon with a 1 cm gap and 0.8 nm wide interference filter. (b) Same as (a) but with a second etalon with a 0.186 cm gap. (c) Same as (b) but with a third etalon with a 0.025 cm gap.

occurs in the upper atmosphere where widely spaced emission lines are viewed against a dim background. The line of interest is isolated by adding a low resolution interference filter. In the lower atmosphere, such as the stratosphere, where we observe absorption lines in scattered sunlight, a single etalon would transmit light through all orders and would overwhelm the signal. It is necessary to use a multiple etalon system in order to reduce this unwanted light.[19,20] If the thicknesses of the etalons are properly chosen,[21] then it is possible to reduce the "parasitic" light of the instrument to an acceptable level. The effect of adding a second and third etalon with an interference filter to the system is shown in Figs. 2(b) and 2(c). The HRDI instrument has one etalon that has a fixed gap of 1.0 cm and is scanned by observing difference angles through the etalon by means of a multi-channel detector. The gaps of the second and third etalons (0.186 and 0.025 cm thickness) can be varied slightly (~1000nm) with piezoelectric materials so that these etalons can be adjusted to be in resonance with any order of the fixed, high resolution etalon. This allows the instrument to be scanned in wavelength over a range which is limited only by the interference filter.

In order to determine winds, which is the primary product of the HRDI instrument, it is necessary to be able to determine the Doppler shift of an absorption or emission line. Here we demonstrate conceptually how this is done, but note that the actual recovery of the Doppler shift is more difficult. The signal, C, observed on channel i in the presence of a shifted emission or absorption line is given by

$$C_i(v) = C_i(0) + (\delta C/\delta v)_i v \tag{5}$$

where v is the velocity. This can be inverted and converted by the Doppler equation to give

$$\begin{aligned} v &= \frac{c[C_i(v) - C_i(0)]}{v(\delta C/\delta v)_i} \\ &= \frac{cC_i(v)}{v(\delta C/\delta v)_i} - \frac{cC_i(0)}{(\delta C/\delta v)_i} = v_{mea} - v_0 \end{aligned} \tag{6}$$

where c is the speed of light, v_{mea} the raw measured position and v_0 the reference or zero position. The statistical uncertainty of velocity can be estimated by assuming the only source of error is photon statistics in $C_i(v)$. This is the largest source of error and can adequately describe the statistical error. By using Poisson statistics which describe photon noise, the uncertainty in v is given by

$$\delta v = \frac{c}{v\sqrt{C}\,\frac{1\delta C}{C\delta v}}\,. \tag{7}$$

This shows that to minimize wind errors, the signal should be as bright as possible and the slope of the signal should be large. The instrumental width (~0.001 nm, 0.02 cm^{-1}) is significantly greater than the shift due to atmospheric winds. It is important to recognize that HRDI measures Doppler shifts on the order of 10^{-5} nm, and is not attempting to resolve spectral features of this magnitude. Since the width of the spectral line depends on convolution of the instrument width and the atmospheric line shape, there is no reason to make the instrument resolution much narrower than the line as the resultant signal will not become sharper and the signal to noise will decrease.

II.B. Description of Instrument

The HRDI instrument consists of three components: a telescope for viewing the atmosphere (Fig. 3), the interferometer (Fig. 4) and the microprocessor and electronics. Light from the atmosphere is collected by a fully gimballed telescope that allows observation on either side of the spacecraft. The telescope is a 17.8 cm diameter off-axis Gregorian design with vertical and horizontal fields of view equal to 0.12° and 1.37°, respectively. Light enters the interferometer either from the telescope or from calibration sources (spectral and incandescent lamps) by positioning a scene selector mirror. The light beam is expanded from 3 mm in diameter to 25 mm and passes through a dual filter wheel. Each filter wheel holds eight filters and each filter has a bandwidth of ~0.8 nm (17 cm^{-1}). A small fraction of the light is collected by a photometer which provides information on the brightness in the broader spectral region. The light beam is then further expanded to 96 mm diameter and passes through the three etalons. The spectrally dispersed beam is focused on the detector by a telescope with folded optics that allows a 2 meter focal length to be incorporated in about a one-half meter space. The detector is a multiple channel concentric ring detector that spatially scans the highest resolution etalon in wavelength. This device, known as an Image Plane Detector (IPD)[22] is a photomultiplier with an anode pattern which duplicates the interference pattern of the interferometer. This allows multiple wavelengths to be simultaneously sampled. For the device used on HRDI, 31 wavelengths are sampled with the spectral width of each channel covering about 0.001 nm. The HRDI instrument is controlled by a dedicated microcomputer. The computer is necessary to properly control the spacing of the piezoelectrically controlled etalon gaps, compensate for thermal drifts, and to point the telescope.

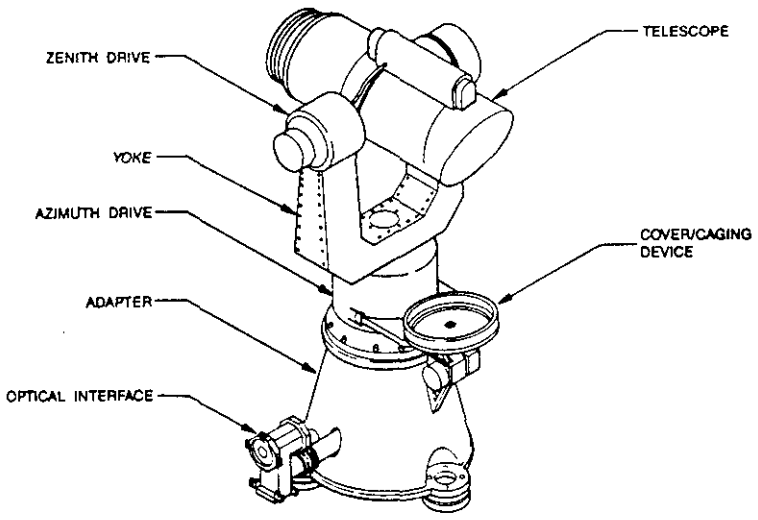

Fig. 3. Drawing of the HRDI telescope. The telescope can rotate around two axes to allow viewing on both sides of the spacecraft and at any altitude in the atmosphere.

III. Mode of Operation

The design of the HRDI instrument allows for versatile programming of operational modes. Here a single mode is described to illustrate the procedure. The operational modes of the instrument are stored in the computer's memory as look-up tables. These tables contain information on the telescope pointing, interferometer tuning wavelength, and dwell time at each altitude. The mode described here is the stratospheric daytime wind mode which scans the stratosphere from 10 to 40 km with a horizonal resolution of ~500 km. The telescope initially looks forward, about 45° to the spacecraft velocity vector, and vertically scans the atmosphere, pausing at each tangent altitude long enough to collect enough signal to meet the required statistical accuracy (see Fig. 5). The telescope scans from the lowest altitude to the highest in the B band and repeats the altitude grid but using the γ band as it scans back down. After this sequence is performed the telescope slews to look backwards, 135° to the velocity vector. The time for the two vertical scans and

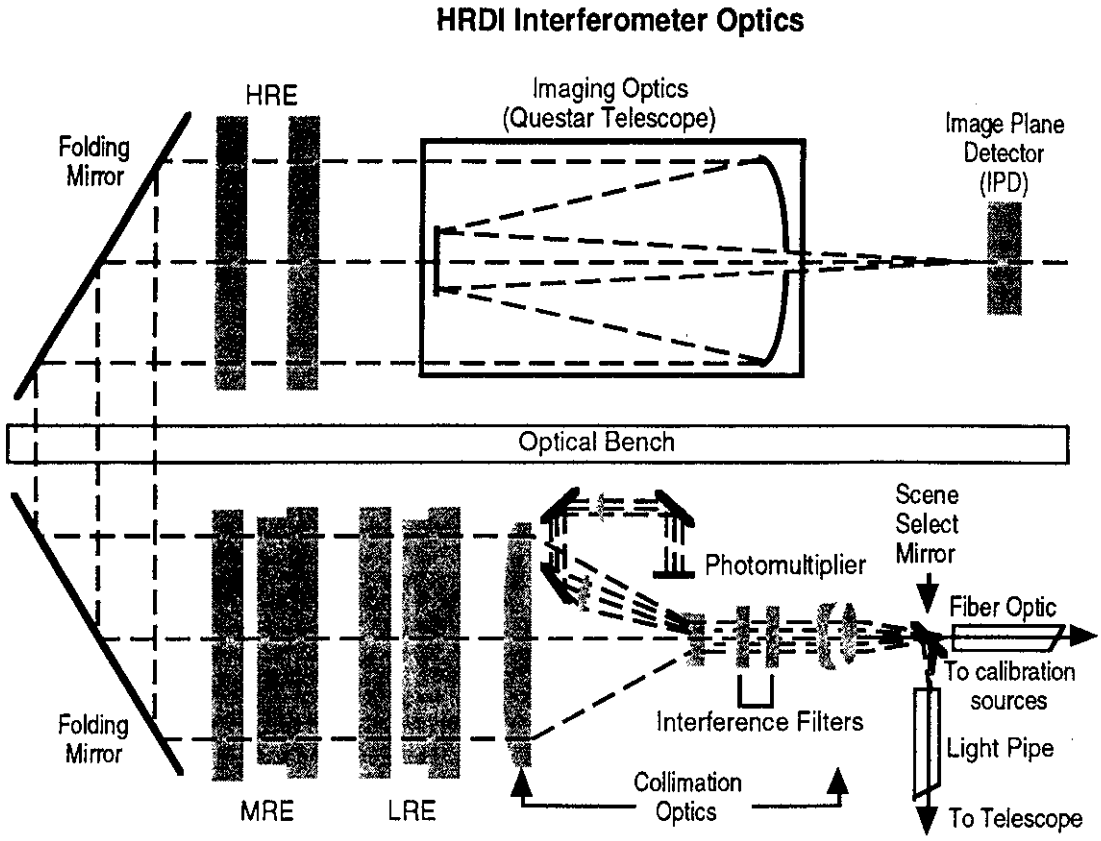

Fig. 4. Optical layout of the HRDI instrument. LRE = low resolution etalon, MRE = medium resolution etalon, HRE = high resolution etalon.

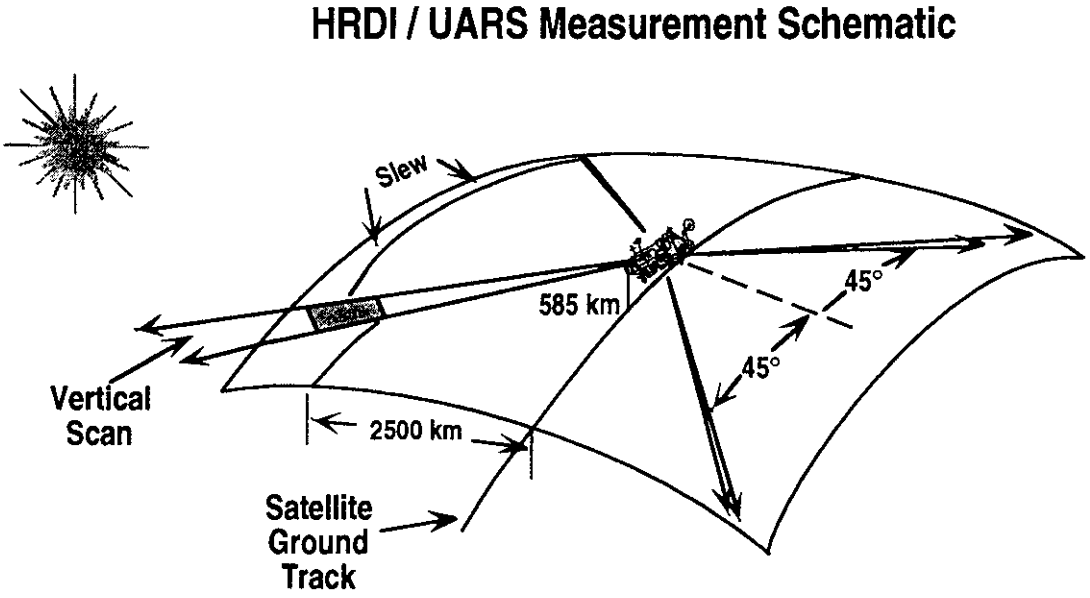

Fig. 5. Illustration of the telescope viewing during a normal science mode. Actual modes will look on just one side of the spacecraft or the other. Typical HRDI operations look on the warm side (towards the sun) to get maximum signal and coverage.

slew is about one minute. The telescope then repeats the two vertical scans and slews back to the forward looking direction. This sequence repeats until the computer issues the commands to start a new mode. With the mode described, a backward viewing scan will sample very nearly the same volume in space as a forward viewing scan performed 9 minutes earlier. The look directions at this volume will differ by 90°, allowing the two measurements to be combined to give a vector.

The data from HRDI consists of a spectrogram of 32 points (31 from the interferometer and one from the photometer channel), the telescope pointing direction and a number of parameters describing the thermal and electrical state of the instrument. All spectrograms from a given altitude are averaged and corrected for instrumental effects. The line of sight Doppler shift is then determined and converted to a line of sight wind speed. Since this represents the integral effect of atmospheric motions, and not a point value, data are then inverted using weighting functions developed by Hays and Abreu.[23] This gives a horizonal component of the wind velocity along a particular look direction. These are combined with measurements from an orthogonal look direction to provide the vector wind at a given point. The result is an altitude stack of wind vectors along the satellite track. Data from other sources (rawinsondes, rockets, etc.) will periodically be used to verify the velocity recovery and provide the zero velocity reference. The final step in the processing is to interpolate the data onto a common UARS spatial and temporal grid for use by the scientific community.

IV. Calibration and Validation

According to Eq. (6), it is necessary to know the reference velocity in order to properly determine the the wind. A number of factors contribute to the determination of v_o, and the most important of these will be discussed here. First, we must know how v_o varies with the state of the instrument. The most important instrument parameters are the length of time in space (because of outgassing) and the instrument mean temperature. The second parameter we need to know is the component of the spacecraft velocity in the look direction. The spacecraft velocity is about 7500 m/s, so even a small uncompenstated component will seriously affect the accuracy of the wind determination. The third piece of knowledge required is the location of the zero wind position. Because of the large Doppler shifts induced by the spacecraft, which has the effect of moving the spectrum around on the detector and because of slight non-uniformities in the detector response, it is not practical to try to locate the zero position during pre-launch calibration. Instead, we use actual wind data collected in orbit. This data is used with geophysical constraints and correlative data taken by rockets, balloons, radars, and lidars to properly locate the zero position. We shall now discuss each of these three items.

The instrument drift (both temporal and thermal) is monitored using observations of onboard spectral lines. The thermal drift is driven by both orbital variations, which amount to ~±0.1 degrees, and by a monthly solar beta cycle which amounts to about ±1 degree. The short term drift is illustrated in Fig. 6, which shows in velocity units the variation in the position of a neon line at 629 nm (14427 cm^{-1}) over a little less then 3 orbits. This demonstrates that orbital variations cause less than a 1 m/s drift in the instrument. Longer term drifts are determined by analysis of daily calibration data. An example of the long term drift is presented in Fig. 7(a), which indicates the instrument drift as observed in calibration data collected since the beginning of the mission. In Fig. 7(b), the data has been corrected for the temperature sensitivity of the instrument, leaving a residual long term drift. The large change during the first 100 days is probably due to effects such as

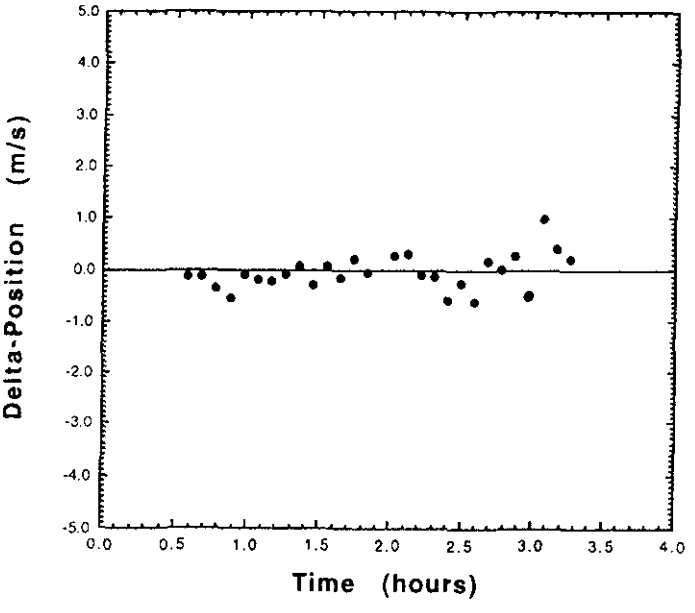

Fig.6. The stability of the HRDI instrument for a short time period, illustrating the lack of sensitivity to orbital variations.

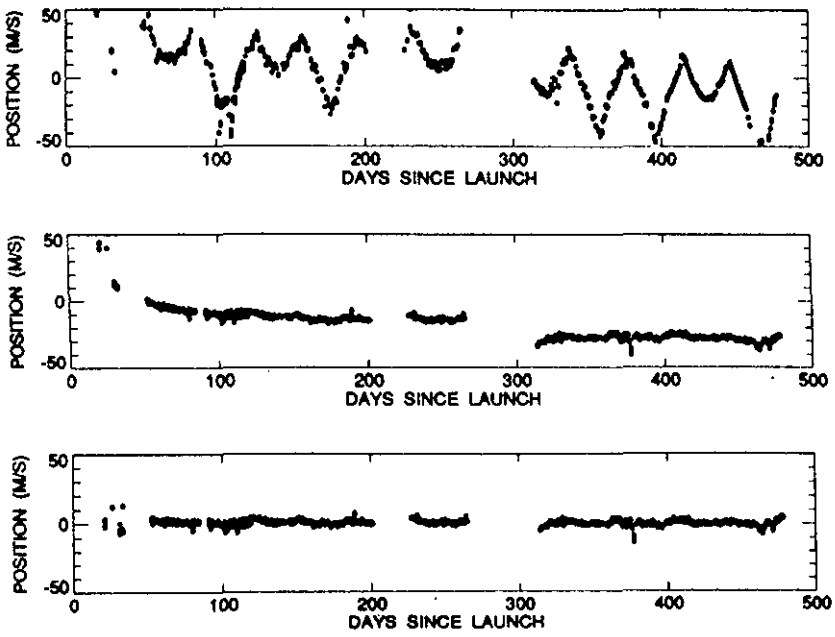

Fig. 7. (a) Position on the HRDI detector in velocity units of the neon calibration line at 14427 cm^{-1}. (b) Position of the calibration line after correction for the temperature sensitivity of the instrument, leaving a residual long term drift. (c) Position of the calibration line corrected for temperature effects and the long term drift. These same corrections are applied to the HRDI atmospheric observations.

outgassing, as the instrument gradually adjusted to the space environment. The area of no data between days 200 and 215 corresponds to a period when there was a partial failure of part of the HRDI electronics and that between days 265 and 310 corresponds to the period when the instrument was powered off due to problems with the spacecraft solar array. There is a substantial shift in line position after this latter period. While the precise cause of this change is still under investigation, it is suspected to have arisen as a result of the extreme low temperatures experienced by HRDI during the extended interval when instrument power was switched off. In any case, the data may be readily corrected for the observed long term drift [Fig. 7(c)]. The temperature variations and the long term drift can be determined to a few meters/second and are used to correct the HRDI observations.

The spacecraft velocity of 7500 m/s is large compared to the typical winds in the atmosphere and so steps must be taken to remove spacecraft effects. The satellite velocity is known to better than 1 m/s, so by itself is not a major source of error. The major source of uncertainty is the location of the telescope viewing direction relative to the satellite velocity vector. A 0.1 degree error in the knowledge of this would typically produce a ~10 m/s error in the wind measurement. The spacecraft attitude is known to about 0.01 degrees, so this is not the source of error. The problem arises from the relationship between the spacecraft reference frame and the telescope frame. This was measured in pre-flight calibrations, but is subject to change due to launch shifts, to relocation in a zero gravity environment, and to differential heating of the spacecraft during the solar beta cycle. The first two of these will be unchanged once orbit is achieved, but the third is time dependent.

The misalignment between the spacecraft frame and the HRDI instrument frame is measured periodically. This is done by observing the passage of stars through the telescope field of view. These measurements are carried out in two ways: in the first, the roll and pitch misalignments are measured by allowing several stars (near the roll/pitch plane and at various angles from the roll axis), to pass through the field of view. We can then determine the difference between the measured crossing time of the star through the field of view and a calculated crossing time based on knowledge of the spacecraft ephemeris and the star's position in the sky. Although each measurement provides only information about the sum of the roll and pitch misalignments, by combining the information from several stars at different angles from the roll axis in a least squares fashion, the roll and pitch errors can be separated.

Because the view of the sky is limited by the spacecraft and by the Earth, it is necessary to use a different technique to determine the yaw misalignment. This involves viewing a series of stars, employing a different offset between each of the expected star positions and the telescope boresight. The presence or absence of a star signature at the various offsets yields the yaw misalignment.

Figure 8 shows our determinations of the misalignments between the HRDI and spacecraft

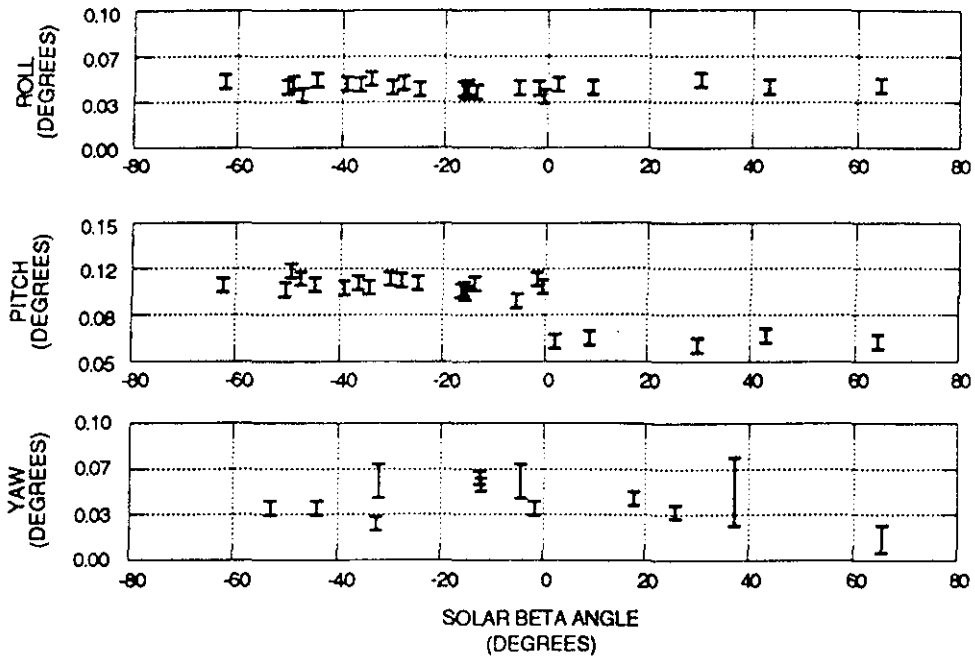

Fig. 8. Determination of the misalignments between the HRDI telescope and the spacecraft coordinate system. The bias in all axes indicate either a launch shift or effect of changing from a 1-g environment to 0-g.

frames. Note that the pitch misalignment changes depending on the sign of the spacecraft beta angle (the angle between the orbit plane and the sun). This result was somewhat surprising at first, but we theorize that the alignment difference is caused by the fact that the spacecraft itself is yawed around 180 degrees when the beta angle changes signs, to keep the sun on the same side of the spacecraft (toward the solar panel and away from the instruments' radiators). These two states of the spacecraft/sun alignment may cause differences in the way the spacecraft structure is heated by the sun, and thus change the misalignment between the spacecraft and the HRDI instrument.

The in-flight calibration data provides information on changes in the zero reference position, but not its absolute value. This parameter is determined from geophysical constraints and correlative data. An example of reasonable geophysical constraints for the mesosphere are that the global mean winds sampled at the same local time do not change rapidly over a period of a day or two and that the long-term global mean meridional winds are zero. The two constraints have yielded estimates of the reference positions accurate to within about 10 ms^{-1}.

Further improvement in the accuracy of the zero reference positions requires the comparison of HRDI measurements with other UARS instruments, particularly the Wind Imaging Interferometer (WINDII), ground based instrumentation (lidars, radars, etc.), special *in situ* measurements (balloons, rockets), and the results of models and climatology. An example of a comparison between winds observed by HRDI with those obtained by a rocket launched from Wallops Island is presented in Fig. 9. It is a non-trivial problem to compare satellite remote sensing observations with other types of data. Correlative instruments typically provide vertical profiles more or less directly above the station, yielding essentially point measurements. In contrast, limb viewing satellite instruments such as HRDI give profiles which are a weighted average along the line of sight. There are also uncertainties associated with the averaging procedures employed by the correlative measurement techniques. Because of the different effective spatial and temporal resolutions of the HRDI and correlative measurements and the high degree of short term atmospheric variability, this means that the various techniques are not really sampling the same quantity. In addition, most inversion methods (including those used by HRDI) employ filtering techniques designed to remove altitude oscillations which are purely artifacts of the analysis procedure. These may have varying degrees of success, and it is possible that variations which are real may be removed from the data.

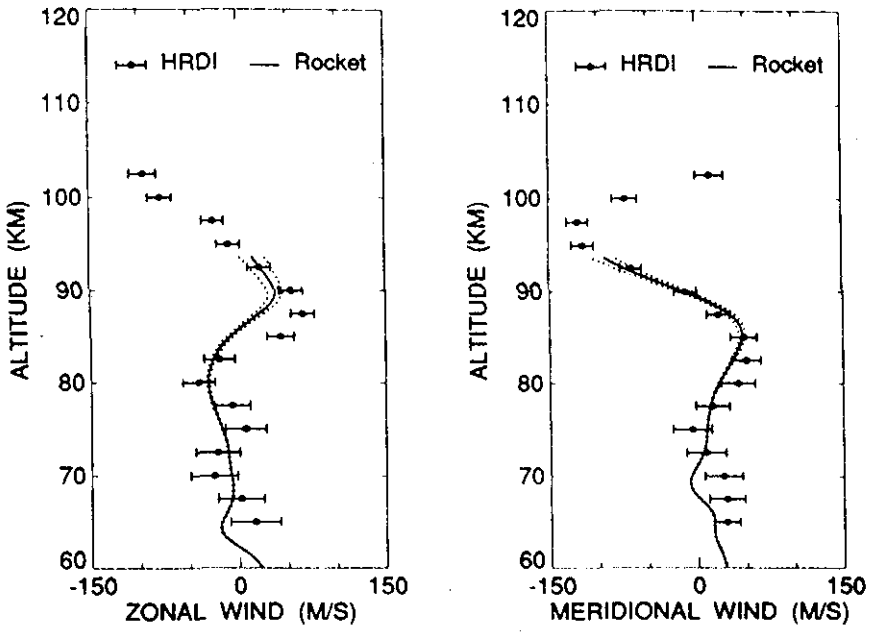

Fig. 9. Wind profiles determined using HRDI at 16:09 UT and a rocket launched from Wallops Island at 16:14 UT on March 25, 1992. The spatial separation between the two sets of measurements was about 300 km, and the solar zenith angle was 40°. The broken lines indicate the uncertainty in the rocket observations.

Another difficulty is that the coincidence of the HRDI and correlative measurement is never exact, either in space or time. Because of the problems outlined above, the comparison of HRDI data with other measurements on a profile by profile basis is of limited value. It is necessary instead to view the data sets from a statistical perspective. One approach is to determine the mean differences between the HRDI and correlative measurements for each site using as many coincidences as possible (typically 10-50). This information allows the zero velocity to be determined to within a few meters per second.

V. Sample Results

HRDI has been collecting data since October, 1991 and here we will show a few examples of the preliminary results. As a matter of convenience, we divide the atmosphere into the lower (stratosphere) and upper (mesosphere and lower thermosphere). This division is based solely on our operational method of collecting data. In the mesosphere we determine the wind field between about 50 and 110 km altitude , the atmospheric temperature and the volume emission rate of the O_2 Atmosphere band during the day and the wind at about 95 km at night. The spectra contain information about the density of O_2 and the concentration of ozone at these altitudes and we are in the process of determining the quality of recovery of these quantities. The stratospheric data contain information on the winds from about 20 km to 40 km with a vertical resolution of 2.5 km. The aerosol extinction coefficient at 630 and 690 nm and the aerosol phase function are also determined. In addition, quantities related to the cloud height and surface albedo are recovered. The horizontal resolution for all of these parameters is a few hundred kilometers along the track and data collection is limited to the daytime portion of the orbit.

Figure 10(a) illustrates a recovered wind field in the mesosphere and lower thermosphere. This shows an averaged meridonal wind field for the month of March, 1991. The data have been averaged over all longitudes and are shown for a local time of 1200 hours. The variations with altitude of the field are the results of the diurnal tide caused by solar heating in the troposphere. In Fig. 10(b) the observations are compared to a tidal simulation.[24] The general structures are the same in both, although the vertical wavelength observed by HRDI (22-25km) is slightly shorter than predicted by the model.

The algorithms for the stratospheric inversions are still under the final stages of development. However, they are at a level sufficient to resolve the gross characteristics of the stratospheric wind field as illustrated in Fig. 11. This shows the wind field on September 7, 1992 at 30 km. The winds at high latitudes are very large, revealing the presence of the polar vortex, which is so important in understanding the ozone chemistry at these latitudes. The use of HRDI data to determine the winds and other UARS instrumentation that measure the constituent densities and temperatures will be used to unravel the complex ozone problem.

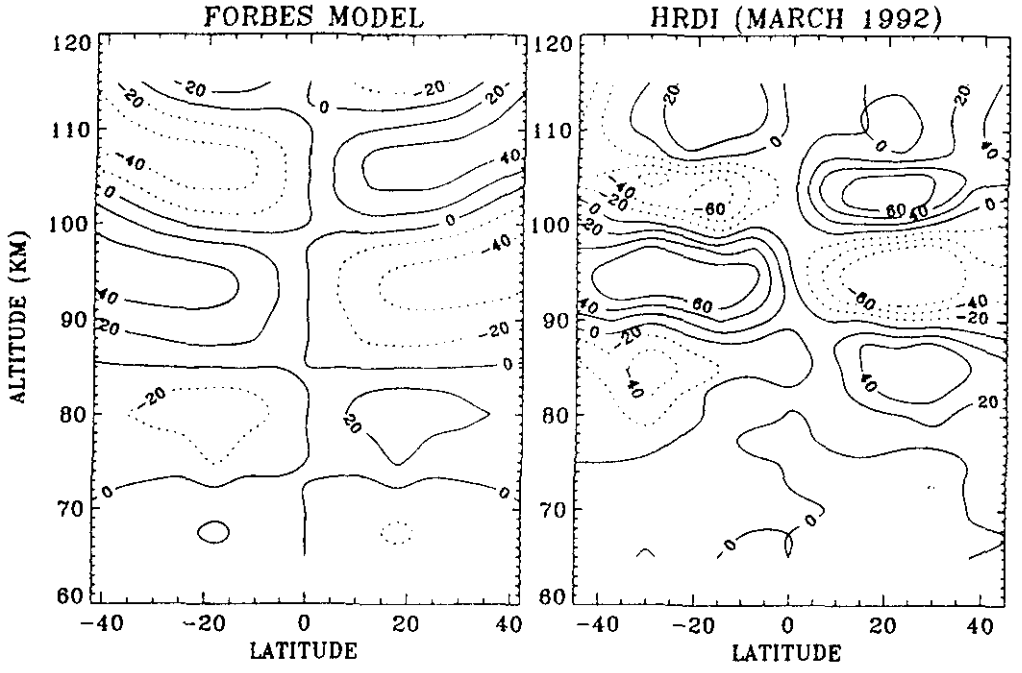

Fig. 10. (a) The mean meridonal wind field (positive towards north) for the month of March, 1991 at a local time of 1200 hours. (b) The meridonal wind field due to a model prediction of the dirunal tide.

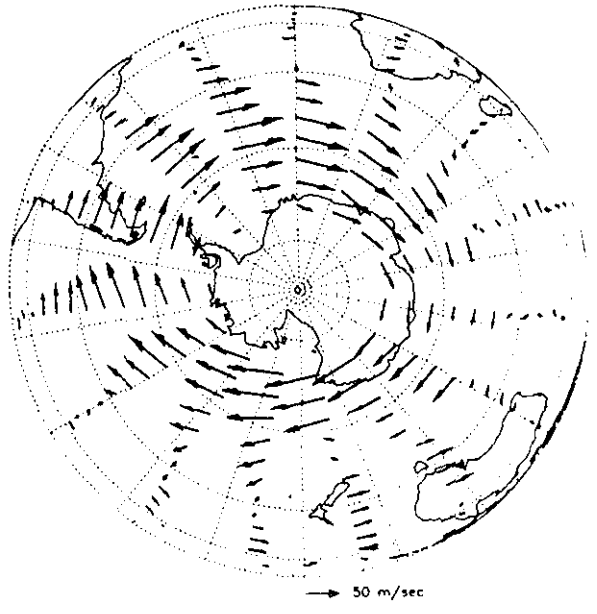

Fig. 11. The wind field at 30 km on September 7,1992 showing the polar vortex in the southern hemisphere winter.

VI. Conclusion

A high resolution, high throughput and extremely stable Fabry-Perot interferometer has been constructed for the direct measurement of Doppler shifts of atmospheric absorption and emission lines. Observations of the winds in the mid-stratosphere, mesosphere and lower thermosphere have been made since October, 1991. Early results show that many of the large scale features are in general agreement with expectations, but there are structures in the wind fields that are not yet understood. Future work will provide new and exciting information about the Earth's middle atmosphere.

VII. References

[1]Andrews, D. J., Holton, J. R. and Leovy, C. B., *Middle Atmosphere Dynamics*, Academic Press, Inc., New York, 1987.

[2]Reber, C. A., "The Upper Atmosphere Research Satellite," *EOS*, Vol. 71, 1990, pp. 1867-1878.

[3]Hays, P. B., "High-Resolution Optical Measurements of Atmospheric Winds from Space. 1: Lower Atmosphere Molecular Absorption," *Applied Optics*, Vol. 21, 1982, pp. 1136-1141.

[4]Abreu, V. J., Bucholtz, A., Hays, P. B., Ortland, D. A., Skinner, W. R., and Yee, J.-H., "Absorption and Emission Line Shapes in the O_2 Atmospheric Bands: Theoretical Model and Limb Viewing Simulations," *Applied Optics,* Vol. 28, 1989, pp. 2128-2137.

[5]Wallace, L., and Hunten, D. M., "Dayglow of the Oxygen A Band," *Journal of Geophysical Research* Vol. 73, 1968, pp. 4813-4834.

[6]Bucholtz, A., Skinner, W.R., Abreu, V. J., and Hays, P. B., "The Dayglow of the O_2 Atmospheric Band System," *Planetary and Space Sciences*, Vol. 34, 1986, pp. 1031-1035.

[7]Lee, L. C., and Slanger, T. G., "Observations on $O(^1D \rightarrow {}^3P)$ and $O_2(b^1\Sigma^+_g \rightarrow X^3\Sigma^-_g)$ Following O_2 Photodissociation," *Journal of Chemical Physics*, Vol. 69, 1978, pp. 4053-4060.

[8]Gauthier, M. J., Snelling, D. R., "Production de $O_2(b^1\Sigma^+_g)$, v'=0, 1, et 2 par la reaction $O(2^1D_2)$ + $O_2(X^3\Sigma^-_g)$," *Canadian Journal of Chemistry*, Vol. 52, 1974, pp. 4007-4015.

[9]Schurath, U., "The Energy Pooling Reaction $2O_2(^1\Delta_g) \rightarrow O_2(X^3\Sigma^-_g) + O_2(b^1\Sigma^+_g)$ Formation, Relaxation, and Quenching of Vibrationally Excited $O_2(b^1\Sigma^+_g)$," *Journal of Photochemistry*, Vol. 4, 1975, pp. 215-226.

[10]Hays, P. B., Skinner, W. R., Abreu, V. J., and Yee, J.-H., "The High Resolution Doppler Imager," in *Digest of the Topical Meeting on Optical Remote Sensing of the Atmosphere*, Optical Society of America, Washington, D.C., 1990, Vol. 4, pp. 7-10.

[11]Abreu, V. J., Hays, P. B., and Skinner, W. R., "The High Resolution Doppler Imager," *Optics & Photonics News*, Vol. 2, #10, 1991, pp. 28-30.

[12]Hays, P. B., Abreu, V. J., Dobbs, M. E., Gell, D. A., Grassl, H. J., and Skinner, W. R., "The High Resolution Doppler Imager on the Upper Atmosphere Research Satellite," to appear in the *The Journal of Geophysical Research - Atmosphere*, Special UARS issue, 1993.

[13]Hays, P. B., and the HRDI Science Team: Abreu, V. J., Burrage, M. D., Gell, D. A., Grassl, H. J., Marshall, A. R., Morton, Y. T., Ortland, D. A., Skinner, W. R., Wu, D. L., and Yee, J.-H., "Remote Sensing of Mesospheric Winds with the High Resolution Doppler Imager," to appear in the Special Bates volume of *Planetary and Space Sciences*, 1993.

[14]Skinner, W. R., Hays, P. B., and Abreu, V. J., "Wind Measurements with a High Resolution Doppler Imager (HRDI)," *Proceedings of the NASA Symposium on Global Wind Measurements*, A. Deepak Publishing, Hampton, VA, 1986, pp. 129-132.

[15]Skinner, W. R., Hays, P. B., and Abreu, V.J., "High Resolution Doppler Imager," IGARSS '87, February, 1987.

[16]Jacquinot, P., "The Luminosity of Spectrometers with Prism, Gratings, or Fabry-Perot Etalons," *Journal of the Optical Society of America*, Vol. 44, 1954, pp. 761-765.

[17]Hernandez, G., *Fabry-Perot Interferometers*, Cambridge University Press, Cambridge, 1986.

[18]Vaughn, J. M., *The Fabry-Perot Interferometer*, Adam Hilger, Bristol, 1989.

[19]Mack, J. E., McNutt, D.P., Roesler, F. L., and Chabbal, R., "The Pepsios Purely Interferometric High-Resolution Scanning Spectrometer. 1. The Pilot Model," *Applied Optics*, Vol. 2, 1963, pp. 873-885.

[20]McNutt, D. P., "Pepsios Purely Interferometric High-Resolution Scanning Spectrometer. II. Theory of Spacer Ratios," *Journal of the Optical Society of America*, Vol. 55, 1965, pp. 288-292.

[21]Skinner, W. R., Hays, P. B., and Abreu, V. J., "Optimization of a Triple Etalon Interferometer," *Applied Optics*, Vol. 26, 1987, pp. 2817-2827.

[22]Hays, P. B., Killeen, T. L., and Kennedy, B. C., "The Fabry-Perot Interferometer on Dynamics Explorer," *Space Science Instrumentation,* Vol. 5, 1981, pp. 395-416.

[23]Hays, P. B., and Abreu, V. J., "Absorption Line Profiles in a Moving Atmosphere: A Single Scattering Linear Perturbation Theory," *Journal of Geophysical Research,*Vol. 94, 1989, pp. 18351-18365.

[24]Forbes, J. M., "Atmospheric Tides 1. Model Description and Results for the Solar Diurnal Componet," *Journal of Geophysical Research*, Vol. 87, 1982, pp. 5222-5240.